Advances in Applied Mathematics and Mechanics
Adv. Appl. Math. Mech., Vol. **6**, No. 3, pp. 307-326

DOI: 10.4208/aamm.2013.m409
June 2014

A Numerical Study of Jet Propulsion of an Oblate Jellyfish Using a Momentum Exchange-Based Immersed Boundary-Lattice Boltzmann Method

Hai-Zhuan Yuan[1], Shi Shu[1], Xiao-Dong Niu[1,2,*], Mingjun Li[1] and Yang Hu[1]

[1] *School of Mathematics and Computational Science, Xiangtan University, Xiangtan 411105, China*
[2] *Department of Mechatronics, College of Engineering, Shantou University, Shantou 515063, China*

Received 19 November 2013; Accepted (in revised version) 17 January 2014

Available online 21 May 2014

Abstract. In present paper, the locomotion of an oblate jellyfish is numerically investigated by using a momentum exchange-based immersed boundary-Lattice Boltzmann method based on a dynamic model describing the oblate jellyfish. The present investigation is agreed fairly well with the previous experimental works. The Reynolds number and the mass density of the jellyfish are found to have significant effects on the locomotion of the oblate jellyfish. Increasing Reynolds number, the motion frequency of the jellyfish becomes slow due to the reduced work done for the pulsations, and decreases and increases before and after the mass density ratio of the jellyfish to the carried fluid is 0.1. The total work increases rapidly at small mass density ratios and slowly increases to a constant value at large mass density ratio. Moreover, as mass density ratio increases, the maximum forward velocity significantly reduces in the contraction stage, while the minimum forward velocity increases in the relaxation stage.

AMS subject classifications: 60-08, 65C20, 68U20

Key words: Lattice Boltzmann method, immersed boundary method, momentum exchange, oblate jellyfish, locomotion.

1 Introduction

It has been generally known that researching fluid-structure-interaction (FSI) problems are become more and more important in engineering applications and biology kinematics. In mechanical engineering, in order to well design the devices (such as aircraft, heart

*Corresponding author.
Email: xdniu@stu.edu.cn (X. D. Niu)

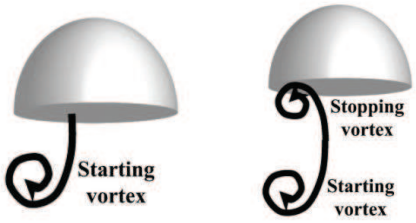

(a) (b)

Figure 1: Schematic of a jetting medusa with vortex rings in the wake [17].

valves, pumps, etc.), fluid-structrue-interaction phenomenas, that play a key role in the dynamic stability of structure, should be required the consideration. Otherwise, the devices can be broken because of the negligence of FSI oscillations. In civil engineering, the FSI investigations should be done as well. Failing to consider the effects of FSI oscillations, many civilian projects (such as bridges, dams, Marine platform etc.) would perhaps lead to disastrous consequences. In biology kinematics, the dynamics of many motions are due to the force generated by FSI (On a macroscopic scale, such as swimming fish, flying birds, falling leaves, and so on. On a mesoscopic scale, including swimming sperms inside the body liquid, red cells in blood, etc.). Where, FSI phenomenas can become more complicated, since the structures are often deformable and involving self motion. The research of motion principle of creatures is significant in military and civil application. For example, the study of insect's flight ability is essential for design of micro air vehicles; Swimmer can benefit from the swimming fish; and so on. In present paper, the research subject is swimming jellyfish to provide an insight into the thrust mechanism.

In the past decades, there have been growing research interests on the dynamics of jellyfish owing to its not overly complex structures [1–17]. Based on intensive experimental investigations [2, 6, 13, 17], the fluid interactions and patterns of flow around the swimming jellyfish have been well described qualitatively. The swimming of the jellyfish depends upon rhythmic contraction and relaxation of their swimming bells. Jet propulsion, as a principal thrust-generating mechanism, is a commonly effective dynamics in the jellyfish swimming. Jet propulsion of the jellyfish generates starting vortex rings (see Fig. 1(a)) in their contraction and produces stopping vortex rings which rotate opposite to the starting vortices (see Fig. 1(b)) in their relaxation. Subsequently, the two kinds of vortex rings interact and develop to azimuthal instabilities as they propagate downstream, which pushes the jellyfish swimming forward. However, flow visualization studies [2, 3, 6, 11, 15] disclose that the jet-propulsion of the jellyfish with more oblate bell has a more complex wake pattern than those with more prolate bell. The kinematic comparison of the jellyfish bell contraction by four species of hydromedusae [16] indicates that the propulsion of the oblate jellyfish is fundamentally different from that of the prolate jellyfish: the oblate jellyfish contracts primarily near the bell margin, and produces a broader, lower velocity jet.

The quantitative characteristics of the flow surrounding of the jellyfish are likely to

be altered by different natural flow parameters [13]. To further understand the propulsion mechanisms of the oblate and prolate jellyfish, numerous theoretical and numerical works have been carried out in recent years [2, 5, 8, 10, 15, 17–19]. A mathematical model to describe the prolate jellyfish was proposed by Colin and Costello [2]. Mchenry and Jed [15] found that a mathematical model to describe the motion of swimming jellyfish should consist of three equations that describe the motion of the margin angle, bell height and bell diameter, respectively.

The swimming of the jellyfish is actually a fluid-structure-interaction (FSI) problem in fluid mechanics. A challenge in the developing numerical models for the jellyfish is to consider the FSI and to obtain quantitatively jellyfish locomotion, including: forward velocity, acceleration, position and force. In this paper, a momentum exchange-based Immersed boundary-lattice Boltzmann method (MEIB-LBM) proposed by Niu et al. [20] is used to study the jet propulsion mechanism of the oblate jellyfish. The present method combines the advantage of the popular lattice Boltzmann method (LBM) [21] and the immersed boundary method (IBM) [22] and employs a Cartesian grid for the LBM solving fluid-flow and a Lagrangian grid for the IBM to determine the moving boundary. The couple of the fluid flow and the boundary are through a distributed force, which is obtained at the Lagrangian points by the momentum exchange of the LBM particles interacting with the immersed boundary and distributed onto the fixed Cartesian grid by adding to the LBM equations. The structure of the oblate jellyfish in the present work is described by a two-dimensional elliptic geometry with a cut in the bottom part as suggested by Herschlag and Miller [12]. To find propulsion mechanisms of the oblate jellyfish, the effects of the flow Reynolds number Re and the mass density ratio of the jellyfish to the carried fluid M are studied.

The rest of this paper is arranged as follows: the governing equations of flow field and the mathematical model of the locomotion of the jellyfish are described in Section 2. In Section 3, the numerical algorithm to solve the present model is given in detailed. Sequentially, in Section 4, detailed numerical investigations and discussions are shown. The characteristics of the locomotion of the jellyfish at Reynolds number $Re = 640$ and mass density ratio $M = 0.1$ are given in Section 4.1, and, the effect of Reynolds numbers on the locomotion of the jellyfish is studied in Section 4.2. Finally, the effect of the mass density ratio on the locomotion of the jellyfish, which is studied firstly in the present works, is given in Section 4.3. In Section 5, the conclusions are shown.

2 Governing equations and the dynamic model of the oblate jellyfish

The swimming of the jellyfish in an incompressible flow can be described by the following Navier-Stokes equations [2, 12]:

$$\rho\Big(\frac{\partial\vec{u}}{\partial t}+\vec{u}\cdot\nabla\vec{u}\Big)=-\nabla p+\mu\Delta\vec{u}+\vec{f}, \tag{2.1}$$

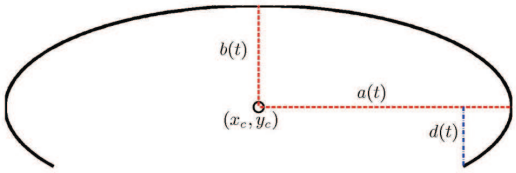

Figure 2: Ellipse to approach the oblate jellyfish.

and

$$\nabla\cdot\vec{u}=0, \tag{2.2}$$

where $\vec{u}$ is the fluid velocity, $p$is the fluid pressure, μ is the fluid viscosity, $\overrightarrow{f}$ is the external force field.

For purely 2D numerical simulations, lots of dynamics models [2,11,12,15,19,23] have been constructed for the real swimming jellyfish. In the present paper, a simple model suggested by Herschlag and Miller [12] is adopted for the present oblate jellyfish and we denote it as H-M model hereafter for a convenience. The H-M model is an elliptic equation used to describe the bell of the jellyfish (see Fig. 2), and it is given as following [12]:

$$\frac{(x-x_c)^2}{a^2}+\frac{(y-y_c)^2}{b^2}=1, \quad y\geq y_c-d, \tag{2.3}$$

where (x_c,y_c) is coordinates of the ellipse center, a is the half width of the bell, b the height of the top part of the bell, d the height of the lower part of the bell.

Motion of the swimming jellyfish in flow filed including two parts: one is self-motion, including contraction and relaxation; another is motion with jet-propulsion. In Self-motion, as the bell geometry of the oblate jellyfish is described by Eq. (2.3), to describe the locomotion of the jellyfish for a fixed time t, we define the parameters a, b, d in Eq. (2.3) as functions of time, and they are [1,12],

$$a(t)=a_0(1-\gamma\cdot p_a), \quad b(t)=b_0(1-\gamma\cdot p_b), \quad d(t)=d_0(1-\gamma\cdot p_d), \tag{2.4}$$

where a_0, b_0 and d_0 are the initial half width of the bell, the initial height of the top part of the bell and the initial height of the lower part of bell, respectively; p_a, p_b and p_d are the percentage changes of the half width of the bell, the height of the top part of the bell and the height of the lower part of the bell, respectively. γ, which also depends on time, is determined by the following equation [12]:

$$\gamma=\frac{1}{2}\left(1+\sin\left(\frac{\pi(2\zeta-1)}{2}\right)\right), \tag{2.5}$$

where, ζ depends on the bell contraction and expansion, it is defined as follows [13,24]:

$$\text{contraction}: \quad \zeta = \frac{t-t_0}{t_c}, \tag{2.6a}$$

$$\text{expansion}: \quad \zeta = 1-\frac{t-t_0}{t_r}, \tag{2.6b}$$

where, t_0 is the start time, t_c is the time cost in the bell contraction stage, and t_r is the time cost in the bell relaxation stage. In Motion with jet-propulsion, Jet-propulsion drives the jellyfish forward. In terms of Newton's second law, the acceleration of the jellyfish is given as:

$$\vec{a}(t) = \frac{\vec{F}_{body}(t)}{\rho_{body} L_{body}}, \tag{2.7}$$

where ρ_{body} is the mass density of the jellyfish, L_{body} is the length of the bell margin, and $\vec{F}_{body}$ is the force acting on the jellyfish calculated by following equation:

$$\vec{F}_{body}(t) = \int_\Gamma \vec{F}(\vec{X}(s,t),t)ds, \tag{2.8}$$

where, $\vec{X}$ is Lagrangian points distributing on the bell, s is the Lagrangian coordinate along the length, Γ represents the surface of the bell, and $\vec{F}(\vec{X}(s,t),t)$ is the external force on the Lagrangian points. $\vec{F}(\vec{X}(s,t),t)$ is computed based on a momentum exchange of the LBM particles interacting with the immersed boundary and will be given in detail in Section 3.3. It should be noted that the gravitational force and the buoyant effect are both neglected in the presented model. The velocity of the jellyfish could be decided by the following equations:

$$\frac{\partial \vec{U}_{body}}{\partial t} = \vec{a}(t). \tag{2.9}$$

3 Numerical algorithm

In the present work, the governing equations (2.1) and (2.2) given in Section 2 are solved by the MEIB-LBM.

3.1 Lattice Boltzmann method for solving flow field

Unlike the continuum fluid equations, the lattice Boltzmann equations are derived from a microscopic kinetics theory. The lattice Boltzmann equations with a single relaxation time under an external force are reproduced here [21]:

$$f_\alpha^*(\vec{x},t) = f_\alpha(\vec{x},t) - \frac{1}{\tau}\left(f_\alpha(\vec{x},t) - f_\alpha^{eq}(\vec{x},t)\right) + F_\alpha \Delta t, \tag{3.1a}$$

$$f_\alpha(\vec{x}+\vec{e}_\alpha\Delta t, t+\Delta t) = f_\alpha^*(\vec{x},t), \tag{3.1b}$$

with

$$F_\alpha = \Big(1-\frac{1}{2\tau}\Big)\omega_\alpha\Big[\frac{\vec{e}_\alpha-\vec{u}}{c_s^2}+\frac{\vec{e}_\alpha\cdot\vec{u}}{c_s^4}\vec{e}_\alpha\Big]\vec{f}, \tag{3.2}$$

where f_α is the density distribution function, f_α^{eq} the equilibrium density distribution function, τ the single relaxation parameter, Δt the size of time step, $\vec{f}$ the external force density as indicated in Eq. (2.1), $\vec{e}_\alpha$ the lattice velocity and ω_α the weight coefficients which depend on the selected lattice velocity model.

In the 2D nine-velocity model (D2Q9), the velocity set is given by

$$\vec{e}_\alpha = \begin{cases} (0,0), & \alpha=0, \\ c\Big(\cos\Big(\frac{\alpha-1}{2}\pi\Big),\sin\Big(\frac{\alpha-1}{2}\pi\Big)\Big), & \alpha=1,3,5,7, \\ \sqrt{2}c\Big(\cos\Big(\frac{2\alpha-1}{4}\pi\Big),\sin\Big(\frac{2\alpha-1}{4}\pi\Big)\Big), & \alpha=2,4,6,8, \end{cases} \tag{3.3}$$

where $c=\Delta x/\Delta t=1$ is the lattice speed, Δx is the lattice spacing. The correspondent equilibrium density distribution function f_α^{eq} can be chosen in the following form:

$$f_\alpha^{eq} = \omega_\alpha\rho\Big[1+\frac{\vec{e}_\alpha\cdot\vec{u}}{c_s^2}+\frac{\big(\vec{e}_\alpha\cdot\vec{u}\big)^2}{2c_s^4}-\frac{\vec{u}^2}{2c_s^2}\Big], \tag{3.4}$$

where $c_s=c/\sqrt{3}$ is the sound speed, $\omega_0=4/9$, $\omega_{1,3,5,7}=1/9$, $\omega_{2,4,6,8}=1/36$, $\vec{u}=(u,v)$ is the velocity of the fluid.

Eqs. (3.1a)-(3.2) approximately recovers the Navier-Stokes equations to the second order based on the Chapman-Enskog expansion, and the corresponding kinematic viscosity v, which is related to the relaxation time τ, is

$$v=c_s^2(\tau-0.5)\Delta t. \tag{3.5}$$

Based on the density distribution function f_α and the external force density $\vec{f}$, the fluid density ρ, velocity $\vec{u}$ are computed as following:

$$\rho=\sum_\alpha f_\alpha, \tag{3.6a}$$

$$\vec{u}=\frac{1}{\rho}\Big(\sum_\alpha\vec{e}_\alpha f_\alpha+\frac{1}{2}\vec{f}\Delta t\Big). \tag{3.6b}$$

3.2 Discrete form of the jellyfish's motion

Considering that, the boundary of the jellyfish is represented by a set of Lagrangian points $\vec{X}(s_l,t)=(X_l(t),Y_l(t))$, $l=1,2,\cdots,np$, (see Fig. 3). To discretize the shape of the jellyfish we set these points satisfy an equal radian distribution, that is:

$$\begin{cases} X_l(t)=x_c(t)+a(t)\cos(\pi+\theta(t)-l\Delta\theta), \\ Y_l(t)=y_c(t)+b(t)\sin(\pi+\theta(t)-l\Delta\theta), \end{cases} \tag{3.7}$$

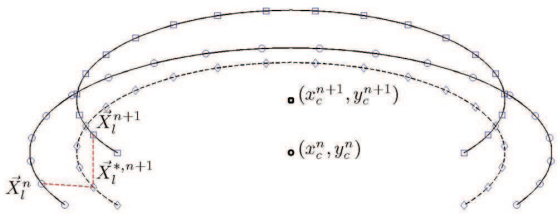

Figure 3: Schematic of jellyfish locomotion ($\vec{X}^n$ is the position of bell at t^n, $\vec{X}^{*,n+1}$ is the position of bell with self motion at t^n, $\vec{X}^{n+1}$ is the position of bell at t^{n+1}).

where $\Delta\theta=\theta(t)/np$ and

$$\theta(t)=\arctan\left(d(t)/\left(a\sqrt{1-d^2/b^2}\right)\right). \tag{3.8}$$

Moreover, $(X_{l+1/2},Y_{l+1/2})$ are the "half-integer" points defined as following:

$$\begin{cases} X_{l+1/2}(t)=x_c(t)+a(t)\cos(\pi+\theta(t)-(l+0.5)\Delta\theta), \\ Y_{l+1/2}(t)=y_c(t)+b(t)\sin(\pi+\theta(t)-(l+0.5)\Delta\theta), \end{cases} \tag{3.9}$$

and the arc length ΔS_l are approximated by:

$$\Delta S_l=\sqrt{(X_{l+1/2}-X_{l-1/2})^2+(Y_{l+1/2}-Y_{l-1/2})^2}, \tag{3.10}$$

Fig. 3 shows the position of the jellyfish updating with one time step. The Lagrangian point $\vec{X}_l$is updated by the following equation

$$\vec{X}_l^{n+1}=\vec{X}_l^n+\vec{d}_{self}+\vec{d}_{body}, \tag{3.11}$$

where $\vec{d}_{self}=\vec{X}_l^{*,n+1}-\vec{X}_l^n$. Obviously, $\vec{X}_l^{*,n+1}$ can be easily computed by Eq. (2.3) and $\vec{d}_{body}=\vec{X}_l^{n+1}-\vec{X}_l^{*,n+1}=\vec{U}_{body}^n\Delta t$ with $\vec{U}_{body}^n$obtained by Eq. (2.9). Then the velocity field $\vec{U}_l^{n+1}$ on the Lagrangian points can be easily obtained as

$$\vec{U}_l^{n+1}=\frac{\vec{X}_l^{n+1}-\vec{X}_l^n}{\Delta t}. \tag{3.12}$$

3.3 A momentum exchange immersed boundary method

In the present simulations, the momentum exchange scheme [20] is adopted to calculate the distributed force produced by the interactions of fluid and the moving boundary of the oblate jellyfish. The density distribution function of the particles on the boundary points at all velocity directions can be approximated

$$f_\alpha(\vec{X},t)=\int f_\alpha(\vec{x},t)\delta(\vec{x}-\vec{X})d\vec{x}, \tag{3.13}$$

where $\delta(\bullet)$ is the non-dimensional Dirac delta function. By using the bounce back rules on the immersed boundary, where the non-slip boundary condition is satisfied, a new set of distribution functions on the boundary points could be computed by

$$f_{-\alpha}^{new}(\vec{X},t)=f_{\alpha}(\vec{X},t)-2\omega_{\alpha}\rho\frac{\vec{e}_{\alpha}\cdot\vec{U}(\vec{X},t)}{c_s^2}, \tag{3.14}$$

where $-\alpha$ denotes the opposite direction of α, i.e., $e_{-\alpha}=-e_{\alpha}$. $\overrightarrow{U}(\overrightarrow{X},t)$ is determined by Eq. (3.12), and ρ could be caculated by Eq. (3.6a) based on $f_{\alpha}(\vec{X},t)$. Then, the force density on the boundary of the jellyfish can be calculated by the momentum exchange concept as following:

$$\vec{F}(\vec{X},t)=\sum_{\alpha}\vec{e}_{\alpha}\left[f_{\alpha}^{new}(\vec{X},t)-f_{\alpha}(\vec{X},t)\right]. \tag{3.15}$$

With Eq. (3.15), the external force density on the flow field can be expressed by:

$$\vec{f}(\vec{x},t)=-\int\vec{F}(\vec{X},t)\delta(\vec{x}-\vec{X}(s,t))ds. \tag{3.16}$$

In the actual implementation, to smooth the Dirac delta function $\delta(\bullet)$, two dimensional distribution functions $D_{i,j}(\vec{x}_{ij}-\vec{X}_l)$ (i, j are the indexes of Eulerian mesh points in x-and y-directions, respectively), which is proposed by Peskin [22] is adopted, that is

$$D_{ij}(\vec{x}_{ij}-\vec{X}_l)=\frac{1}{h^2}\delta_h\Big(\frac{x-X_l}{h}\Big)\delta_h\Big(\frac{y-Y_l}{h}\Big), \tag{3.17}$$

with

$$\delta_h(r)=\begin{cases}\frac{1}{4}\Big(1+\cos\Big(\frac{\pi r}{2}\Big)\Big), & r<2,\\ 0, & r\geq 2,\end{cases} \tag{3.18}$$

where $h=\delta x$ is the mesh spacing.

Thus, the discrete forms of Eqs. (3.13) and (3.16) are

$$\vec{f}(\vec{x}_{i,j},t)=-\sum_{l}\vec{F}(\vec{X}_l,t)D_{ij}(\vec{x}_{ij}-\vec{X}_l)\Delta S_l, \tag{3.19a}$$

$$f_{\alpha}(\vec{X}_l,t)=\sum_{ij}f_{\alpha}(\vec{x}_{ij},t)D_{ij}(\vec{x}_{ij}-\vec{X}_l)h^2. \tag{3.19b}$$

The numerical implementation of the present model with MEIB-LBM for the present swimming of the oblate jellyfish can be illustrated as follows:

Step 1 IBM process to compute the external force density $\vec{F}(\vec{X}_l,t)$ and $\vec{f}(\vec{x},t)$;

Step 1.1 Compute the density distribution functions $f_{\alpha}(\vec{X}_l,t)$ on the boundary using Eq. (3.19b);

Step 2.2 Apply the bounce-back rule on the boundary points using Eq. (3.14) to obtain a new set of distribution functions $f_\alpha^{new}(\vec{X}_l,t)$ on the boundary;

Step 3.3 Compute the external force density $\vec{F}(\vec{X}_l,t)$ on the jellyfish bell using Eq. (3.15);

Step 4.4 Distribute the reacting forces of $\vec{F}(\vec{X}_l,t)$ on the Eulerian points of the flow field with Eq. (3.19a) to obtain the external force density $\vec{f}(\vec{x},t)$ for the flow field.

Step 2 LBM process to update the density distribution functions $f_\alpha(\vec{x},t)$ and the velocity field $\vec{u}(\vec{x},t)$;

Step 2.1 Compute the post-collision density distribution functions $f_\alpha^*(\vec{x},t)$ using Eq. (3.1a);

Step 2.2 Stream $f_\alpha^*(\vec{x},t)$ using Eq. (3.1b) to update the $f_\alpha(\vec{x},t)$;

Step 2.3 Compute the macroscopic fluid density and velocity with the force term $\vec{f}(\vec{x},t)$ according to Eqs. (3.6a) and (3.6b).

Step 3 Update the position $\vec{X}_l(t)$ of the jellyfish and the corresponding velocity $\vec{U}(\vec{X}_l,t)$ by Eqs. (3.11) and (3.12);

Step 4 Repeat Steps 1 to 3 until the convergence criterion is satisfied.

4 Numerical results and discussion

The accuracy and effectiveness of MEIB-LBM has been well demonstrated in our previous works for the fluid-solid [20] and fluid-flexible structure interactions [28]. In the present study, in order to model the contraction and relaxation of the swimming oblate jellyfish as accurate as possible, the parameters of its bell geometry are used as the same as those in [12] and the values are given in Table 1. Those data are obtained by least square fitting the measured representative kinematic profiles of the oblate jellyfish [12]. For convenient simulations and discussions, we define the mass density ratio of the jellyfish to the carried fluid as $M=\rho_{body}/\rho_{fluid}$. The characteristic length of the bell of the oblate jellyfish is defined as $L=2a_i$, and the characteristic velocity of the oblate jellyfish is defined as the average velocity of the tip of jellyfish in the contraction phase by $U=\sqrt{(a_0p_a)^2+(b_0p_b)^2}/t_c$. With defined characteristic length and velocity, the Reynolds number can be easily calculated by $Re=UL/v$ with v the fluid kinematic viscosity. In order to compare the presented study with the previous works, the kinematic viscosity of the fluid is chosen as that in [25], which is $v=1.05\times10^{-6}\text{m}^2/\text{s}$ at the room temperature 20°C for the sea water. In our numerical simulations, the parameters of the fluid are also listed in Table 1 for easy reference. The periodic boundary condtion is used on the fluid domain. The height of fluid domain is set to 0.4m, which makes sure that the

Table 1: Parameters in our numerical simulations.

Jellyfish	Half width (a_0)	0.051m
	Height of top part (b_0)	0.0211m
	Height of lower part (d_0)	0.001759m
	Percentage change of a_0 (p_a)	0.3103
	Percentage change of b_0 (p_b)	0.25
	Percentage change of d_0 (p_d)	-3.0
	The cost time of contraction (t_c)	0.63s
	The cost time of relaxation (t_r)	0.189s
	Mass density (ρ_{body})	0.1
Fluid	Width of fluid domain	0.3m
	Height of fluid domain	0.4m
	Reynolds number (Re)	640
	Density (ρ_{fluid})	1

swimming jellyfish stays inside the domain during all the contraction-relaxation cycles (in our numerical simulations, the maximum number of contraction-relaxation cycles is 7).

4.1 Validation of numerical algorithm

We defined the Strouhal number St as following [12],

$$St = \frac{fD_s}{\overline{U}}, \tag{4.1}$$

where $f = 1/4t_c$ is the frequency of the jellyfish motion, $D_s = a_0(1-p_a)$ is the width of the jellyfish in the fully contracted state, and $\overline{U}$ is the average forward velocity. Obviously, in our numerical simulations, $f$and D_s are constants, that is to say St^{-1} is simply proportional to $\overline{U}$.

The total work W, which is used to evaluate the amount of work generated by the locomotion of the jellyfish, is defined as [12],

$$W = \sum_{n=1}^{nt}\sum_{l=1}^{np} \vec{F}_l^n \Delta S_l^n \Delta \vec{X}_l^n, \tag{4.2}$$

where F_l^n is the force per unit length at Lagrangian boundary point l and discrete time n, nt is the total number of time steps, and ΔX_l^n is the displacement of Lagrangian boundary point l at time n. The total work is normalized by $\rho U^3/2$ in the following numerical results.

In order to make sure that the present algorithm is stable and convergence, four grid sizes are examined: $h = 1/400, 1/600, 1/800, 1/1000$, correspondingly, the number of Lagrangian points are $np = 71, 108, 143, 181$. In general, $Re = 32$ and $M = 0.1$ are considered. Based on the numerical results, the reciprocal of Strouhal number and the total work at

Table 2: The reciprocal of Strouhal number and the total work at different grid sizes.

	(h,np)	St^{-1}	W
Present	$(1/400,71)$	0.0900	0.0490
	$(1/600,108)$	0.1014	0.0461
	$(1/800,143)$	0.1080	0.0449
	$(1/1000,181)$	0.1124	0.0443
Ref. [12]		0.1835	0.0483

different grid sizes are presented in Table 2, which indicate that the presented algorithm is stable and convergent. Furthermore, the total work is consistent with the results presented in [12]. Although the reciprocal of Strouhal number has a certain deviation comparing with the result given in [12], that can be attributed that differences of numerical algorithms and the effect of mass density considered in the presented numerical simulations. That is to say, the presented algorithm can well simulate the jellyfish locomotion.

4.2 Characteristics of the oblate jellyfish locomotion at $Re=640$ and $M=0.1$

4.2.1 Quantifications of oblate jellyfish locomotion

To measure quantifications of the bell during the pulsation cycle, the instantaneous fineness ratio $F(t)$ is defined as [8,11]

$$F(t)=\frac{b(t)+d(t)}{2a(t)}. \tag{4.3}$$

Eq. (4.3) indicates that the fineness ratio $F(t)$ reaches the minimum value at the bell full relaxation, whereas the maximum ratio corresponds to the bell full contraction. Based on the parameters of geometry given in the Table 1, the representative kinematic locomotion of the jellyfish over time, including changes of fineness ratio, displacement, forward velocity and acceleration, is shown in Fig. 4, in which the narrow region denotes the contraction state and the broad region is the relaxation state.

As shown in Fig. 4, the velocity of the oblate jellyfish varies with a similar frequency of the fineness ratio: both increases in contraction state and decreases in relaxation state. The numerical results given by Herschlag et al. [12] were also included in this figure for comparison. Negative velocities in the relaxation state are observed. At the beginning of the first contraction phase, the acceleration reaches a maximum value, and then it decreases rapidly to a minimum value in the contraction state. Since this contraction results in jet propulsion, the jellyfish is pushed forward. The maximum velocity is achieved when the acceleration reaches to zero before the full contraction state. In each contraction, the locomotion displacement of the jellyfish increases rapidly. In the relaxation state, it can be broken down into two stages: firstly, acceleration is in the form of oscillatory nearly a certain value less than zero, so forward velocity decreases continuously. In physics, this is reasonable at the beginning of several cycles as seen in Fig. 5

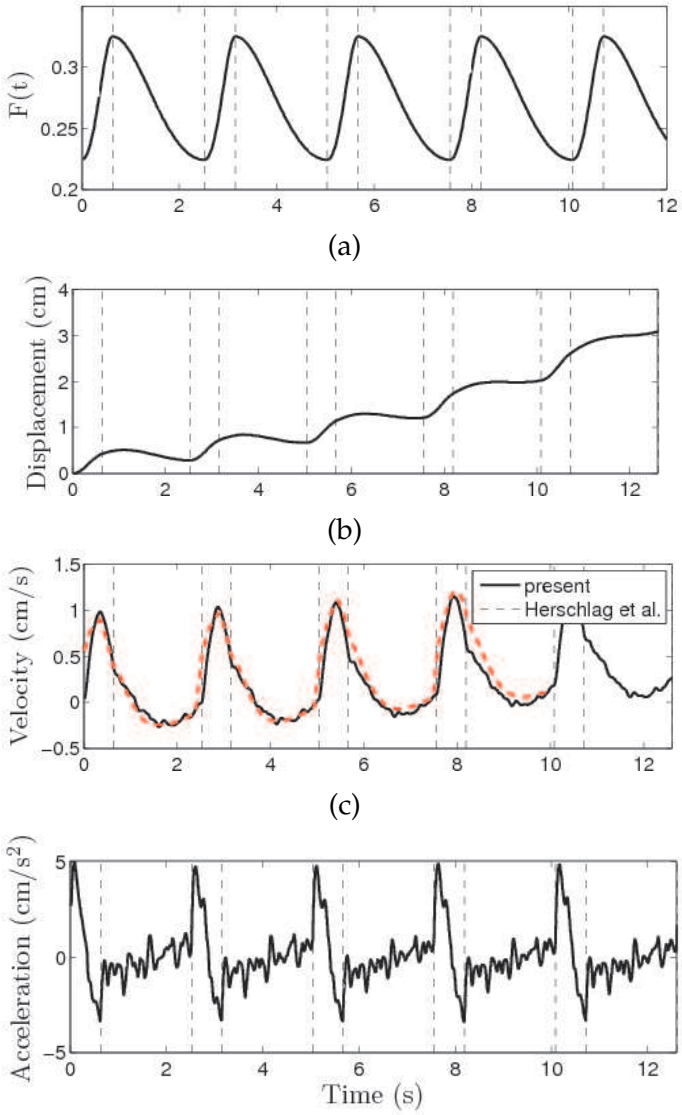

Figure 4: Representative kinematic profiles of oblate jellyfish (the narrow region: the contraction state; the broad region: the relaxation state).

which shows that the jellyfish moves backward. After that, the acceleration is in the form of oscillatory nearly a certain value larger than zero and the forward velocity increase again. It could be found that the locomotion displacement of the oblate jellyfish changes little in the relaxation state. The above results presented in Fig. 4 are agreed fairly well with the previous results obtained in laboratory experiments [3,7,26].

4.2.2 Flow patterns

Vorticity plots of the fluid surrounding the oblate jellyfish during the first swimming cycle are shown in Fig. 5. In the contraction (Frames at 0.158, 0.315 and 0.473s), two starting vortex rings are gradually formed due to the bell contracted. Obviously, the starting vortex rings induce a fluid motion both inside and outside the bell, which was also observed by Dabiri et al. in [1]. As shown in Fig. 5, the velocity vectors directly show that the flow is ejected into the bell cavity to push the bell to move forward. In the full contraction stage (Frame at 0.63s), the starting vortex rings fully formed. Subsequently, two stopping vortex rings are gradually formed inside the bell cavity in the relaxation stage (Frames at 1.1, 1.58 and 2.05). Further observing the corresponding velocity vectors around the stopping vortex rings, it is found that the stopping vortex rings not only induce the flow ejected into the bell cavity, but also interacte with the starting vortex rings. Moreover, the velocity vectors in the stopping vortex rings show that a portion of the fluid in the stopping vortex rings is ejected into the bell cavity, and others joins together with starting vortex rings and then forms larger downstream lateral vortexes. These phenomena are also observed in [1]. Finally, in the full relaxation stage (Frame at 2.52s), two starting vortex rings and two stopping vortex rings are fully formed. This process makes the jellyfish moving forward.

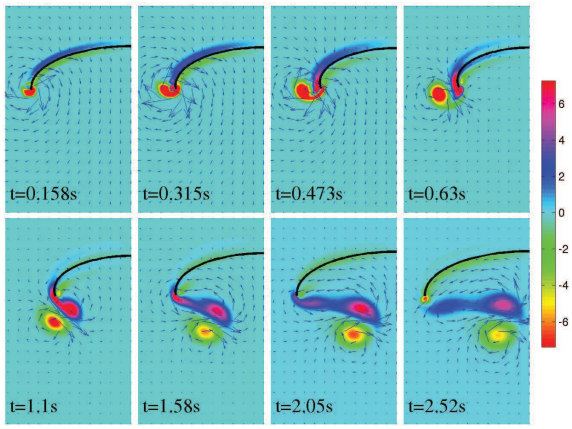

Figure 5: Vorticity plots and velocity vectors of the fluid surrounding the jellyfish during the first swimming cycle (Frames at 0.158s, 0.315s and 0.473s show the process of contraction; Frame at 0.63s shows the full contraction phase; Frames at 1.1s, 1.58s and 2.05s shows the process of relaxation; Frame at 2.52s shows the full relaxation phase).

To present the whole evolutions of the locomotion of the oblate jellyfish, vortex contours at full contraction and relaxation phase of four swimming cycles are plotted in Fig. 6. In the full contraction (Frames at 0.63s, 3.15s, 5.67s and 8.19s), there are always two starting vortex rings formed at the bell margin. In the full relaxation (Frames at 2.52s, 5.04s, 7.56s and 10.1s), these two vortexes are just below the bell and move downward. Particularly, it is found that the later starting vortex rings move faster than the

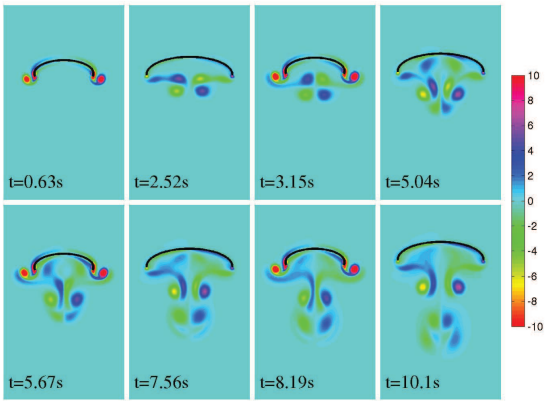

Figure 6: Vorticity plots of the fluid surrounding the jellyfish during the first four swimming cycle (Frames at 0.63s, 3.15s, 5.67s and 8.19s shows the four full contraction phases; Frames at 2.52s, 5.04s, 7.56s and 10.1s shows the four full relaxation phases).

former ones, because that the former vortex induces the downstream fluid that could accelerate the later ones, until they mix together and become larger and more complicated structure. All above results agree well with the experimental visualizations conducted by Dabiri et al. [6], and show that the vortex structures play an important role during the propulsive cycle.

4.3 Effect of Reynolds numbers

4.3.1 Comparing quantifications with different Reynolds numbers

To compare average forward velocity with Reynolds numbers, there are numerical simulations at different Reynolds numbers, and mass density ratio M is always fixed as 0.1. Fig. 7(a) shows the inverse Strouhal number over six cycles at different Reynolds numbers. From this figure, it could be found that the inverse Strouhal number St^{-1} keeps constant in the range of $64 < Re < 160$. And when $Re < 64$, St^{-1} increases linearly with $\log(Re)$. As Re approaches to zero, St^{-1} is also approaches to zero, implying that the average forward velocity also approaches zero, which is consistent with the predictions of the Scallop Theorem: the reciprocal methods of locomotion not working in Stokes flow ($Re \approx 0$) [27]. It is more interesting to find that St^{-1} increases linearly with $\log(Re)$ again when $Re > 160$, and St^{-1} increases more quickly than that at low Reynolds numbers. This result is consistent with the numerical results presented in [12]. The total work done over six cycles is plotted in Fig. 7(b). Note that, for low Reynolds numbers, the total work W, which is put into the pulsations, rapidly decreases with Re increasing. After that, W changes little at $64 < Re < 160$. When $Re > 160$, the total work W slowly increases with Re. These results shown in Fig. 7(b) are accordance with those presented in [12].

For different Reynolds numbers, the locomotion displacement of the oblate jellyfish varies at first five cycles is plotted in Fig. 8(a). It is found that the jellyfish moves rapidly

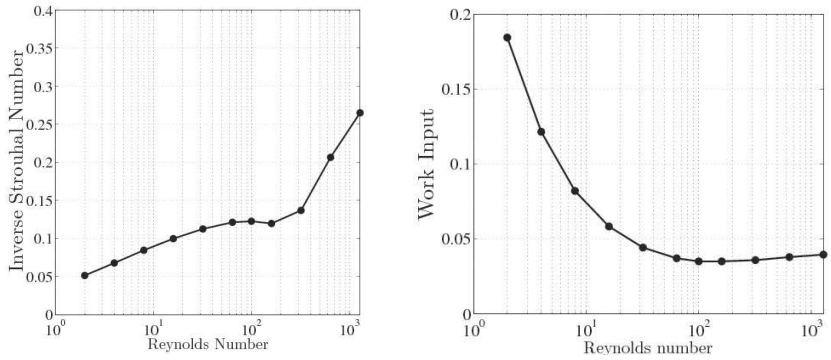

(a) (b)

Figure 7: (a) Inverse Strouhal Number St^{-1} and (b) the work input W at different Reynolds Numbers.

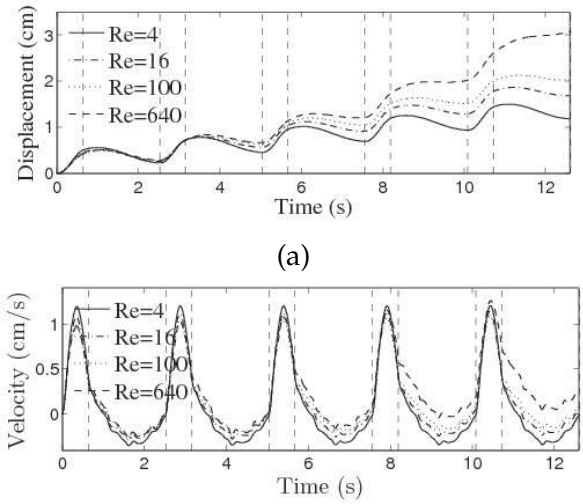

(a)

(b)

Figure 8: Numerically predicted jellyfish (a) displacement and (b) forward velocity at different Reynolds Numbers.

in the contraction and remains standstill in the relaxation. For the low Reynolds numbers $Re=4$, the locomotion displacement of the jellyfish always moves backward in the relaxation stage, while which only appeared at the beginning of several cycles for $Re>16$. Moreover, as the Reynolds numbers increases, the number of cycle decreases. For large Reynolds numbers, especially for $Re\geq 640$, the jellyfish moves faster and faster as time pasts. Fig. 8(b) shows the forward velocity varying with time at different Reynolds numbers. The forward velocity is almost the same in the contraction stage, while it has a significant difference in the relaxation stage. In the relaxation stage, the forward velocity is always negative for the small Reynolds numbers $Re=4$, and as Re increases, the forward velocity increases significantly. That is to say, Reynolds number has a significant

effect on the locomotion of the jellyfish in the relaxation stage.

4.3.2 Influence on flow pattern

Fig. 9 shows vorticity plots of the swimming oblate jellyfish after four cycles for $Re=$ 64,160,640, and 1280, respectively. Vorticity in the wake of the jellyfish quickly dissipates for lower Re, which are the same as predictions in [12]. As Re increases, there are more vortices forming behind the bell, especially for large Reynolds number $Re=1280$, small vortices form in the bell. These vortices play an important role for the movement of the oblate jellyfish.

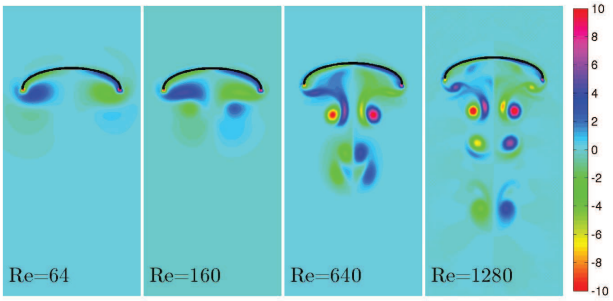

Figure 9: Flow pattern at time 10.1s for different Reynolds Numbers.

4.4 Effect of mass density ratio

4.4.1 Effect of mass density ratio comparing quantifications with different mass density ratios

In order to study effect of mass density ratio, Reynolds number Re is always fixed as 640. Fig. 10(a) shows the inverse Strouhal number over six cycles at different mass density ratios. From this figure, it is found that, for $M<0.1$, as M increases, the inverse Strouhal number St^{-1} increases. However, when $M\geq 0.1$, the inverse Strouhal number St^{-1} decreases with increasing M, and it approach to 0.05 at $M=1$. The total work done over six cycles is plotted in Fig. 10(b). Note that, for small M, the total work rapidly increases with increasing M. And for large M, the total work W slowly increases and the value close to 0.035 finally.

For different mass density ratios, the displacement of the swimming jellyfish varied at first five cycles is shown in Fig. 11(a). When $M=0.01$, the swimming jellyfish always moves backward in the relaxation stage, while which only appeared at the beginning of several cycles for $M\geq 0.1$. And more, as the mass density increases, the number of cycles decreases. Also, the jellyfish moves forward more and more slowly when M increases. Fig. 11(b) shows the forward velocity varying with time at different M. The effect of M on the forward velocity is different to that of Re. M has a significant effect on both the bell relaxation and contraction. As M increases, the maximum forward velocity significantly

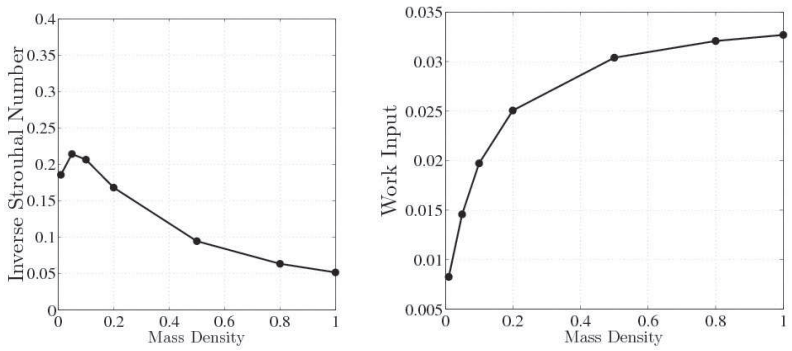

(a) (b)

Figure 10: (a) Inverse Strouhal Number St^{-1} and (b) the work input W at different mass density.

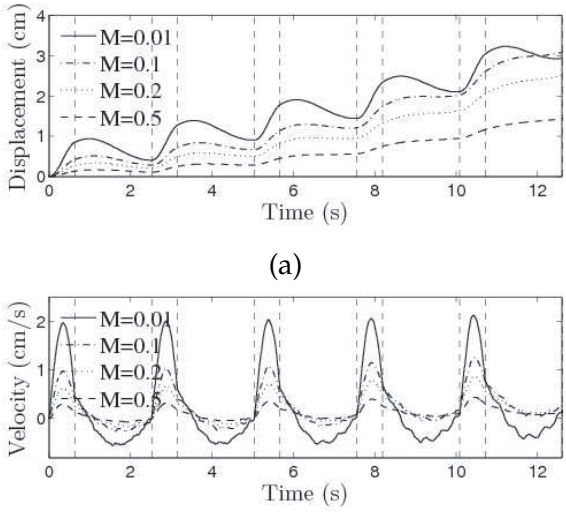

(a)

(b)

Figure 11: Numerically predicted jellyfish (a) displacement and (b) forward velocity at mass density.

decreases in the contraction stage, while the minimum forward velocity increases in the relaxation stage, and more and more close to zero, that is to say, the velocity changes more and more smoothly.

4.4.2 Influence on flow pattern

Fig. 12 shows vorticity plots of the swimming oblate jellyfish after four cycles for $M =$ 0.01,0.1,0.5, and 1. Vorticity in the wake of the oblate jellyfish quickly dissipates for smaller M. As M increases, there are more vortices forming behind the bell, and the vortices become larger. In particular, for mass density $M = 1$, the width of vortices is approach to the width of bell.

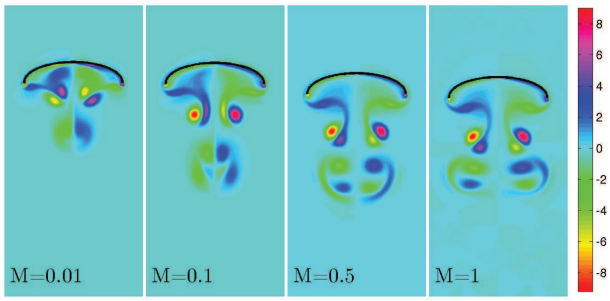

Figure 12: Flow pattern at time 10.1s for different mass density ratio.

5 Conclusions

In present paper, based on the H-M model describing the structure of the oblate jellyfish, a numerical investigation of the locomotion of the oblate jellyfish is carried out by using the MEIB-LBM. In particular, the kinematic profiles of the oblate jellyfish, the effect of Reynolds number and mass density of jellyfish are studied. The numerical results are agreed fairly well with the previous findings obtained in laboratory experiments.

It is found that the velocity has an oscillatory vary with a similarly pattern of the fineness ratio, increasing in the bell contraction and negative velocities are observed in the bell relaxation stage. The locomotion displacement of the jellyfish changes little in the bell relaxation. By comparing average forward velocity and the total work at different Reynolds numbers, it is found that Re has a significant effect on the locomotion of the jellyfish. As Reynolds numbers Re increases, the inverse Strouhal number increases and the total work, which is put into the pulsations, decreases. The forward velocity is almost the same in the bell contraction, which is different to that in the relaxation stage. The inverse Strouhal number St^{-1} increases and decreases before and after $M=0.1$. The total work undergoes a rapid and slow increment at the small and large M, and the value is close to 0.035 finally. Moreover, M has significant effects on both the bell relaxation and contraction. As M increases, the maximum forward velocity significantly reduces in the contraction stage, while, the minimum forward velocity increases in the relaxation stage, and more and more close to zero. Vorticity in the wake of the jellyfish quickly dissipates for smaller M, As M increases, there are more vortices forming behind the bell, and the vortices become larger.

Acknowledgements

This study was supported by the One Hundred Person Project of Hunan Province of China under Xiangtan University, and the Academic Frontier Research Project on "Next Generation Zero-emission Energy Conversion System" of Ministry of Education, Culture, Sports, Science and Technology of Japan, and NSFC Project (Grant No. 91130002

and 11171281), and Innovative Research Team in University of China (No. IRT1179), and Specialized research Fund for the Doctoral Program of Higher Education (Grant No. 20124301110003), and Hunan Provincial Innovation Foundation for Postgraduate (CX2012B239).

References

[1] J. O. DABIRI, S. P. COLIN, J. H. COSTELLO AND M. GHARIB, *Flow patterns generated by oblate medusan jellyfish: field measurements and laboratory analyses*, J. Experimental Bio., 208(7) (2005), pp. 1257–1265.

[2] S. P. COLIN AND J. H. COSTELLO, *Morphology, swimming performance and propulsive mode of six co-occurring hydromedusae*, J. Experimental Bio., 205(3) (2002), pp. 427–437.

[3] J. H. COSTELLO AND S. P. COLIN, *Morphology, fluid motion and predation by the scyphomedusa Aurelia aurita*, Marine Bio., 121 (1994), pp. 327–334.

[4] J. H. COSTELLO AND S. P.COLIN, *Flow and feeding by swimming scyphomedusae*, Marine Bio., 124 (1995), pp. 399–406.

[5] J. O. DABIRI AND M. GHARIB, *Sensitivity analysis of kinematic approximations in dynamic medusan swimming models*, J. Experimental Bio., 206(20) (2003), pp. 3675–3680.

[6] J. O. DABIRI, M. GHARIB, S. P. COLIN AND J. H. COSTELLO, *Vortex motion in the ocean: in situ visualization of jellyfish swimming and feeding flows*, Phys. Fluids, 17(9) (2005), pp. 091108.

[7] J. E. HIGGINS, M. D. FORD AND J. H. COSTELLO, *Transitions in morphology, nematocyst distribution, fluid motions, and prey capture during development of the scyphomedusa cyanea capillata*, The Biological Bulletin, 214(1) (2008), pp. 29–41.

[8] D. RUDOLF AND D. MOULD, *Interactive jellyfish animation using simulation*, in: GRAPP'09, 2009, pp. 241–248.

[9] K. E. FEITL, A. F. MILLETT, S. P. COLIN, J. O. DABIRI AND J. H. COSTELLO, *Functional morphology and fluid interactions during early development of the scyphomedusa aurelia aurita*, The Biological Bulletin, 217(3) (2009), pp. 283–291.

[10] M. DULAR, T. BAJCAR AND B. ŠIROK, *Numerical investigation of flow in the vicinity of a swimming jellyfish*, Eng. Appl. Comput. Fluid Mech., 3(2) (2009), pp. 258–270.

[11] D. RUDOLF AND D. MOULD, *An interactive fluid model of jellyfish for animation*, in: A. Ranchordas, J. Pereira, H. Araújo, J. Tavares (Eds.), Computer Vision, Imaging and Computer Graphics, Theory and Applications, Vol. 68 of Communications in Computer and Information Science, Springer Berlin Heidelberg, (2010), pp. 59–72.

[12] G. HERSCHLAG AND L. MILLER, *Reynolds number limits for jet propulsion: a numerical study of simplified jellyfish*, J. Theoretical Bio., 285(1) (2011), pp. 84–95.

[13] K. KATIJA, W. T. BEAULIEU, C. REGULA, S. P. COLIN, J. COSTELLO AND J. O. DABIRI, *Quantification of flows generated by the hydromedusa aequorea victoria: a lagrangian coherent structure analysis*, Marine Ecology Progress Series, 435 (2011), pp. 111–123.

[14] M. SAHIN, K. MOHSENI AND S. P. COLIN, *The numerical comparison of flow patterns and propulsive performances for the hydromedusae sarsia tubulosa and aequorea victoria*, J. Experimental Bio., 212(16) (2009), pp. 2656–2667.

[15] M. J. MCHENRY AND J. JED, *The ontogenetic scaling of hydrodynamics and swimming performance in jellyfish (aurelia aurita)*, J. Experimental Bio., 206(22) (2003), pp. 4125–4137.

[16] M. FORD AND J. COSTELLO, *Kinematic comparison of bell contraction by four species of hydromedusae*, Scientia Marina, 64 (2000), pp. 47–53.

[17] J. O. DABIRI, *On the estimation of swimming and flying forces from wake measurements*, J. Experimental Bio., 208(18) (2005), pp. 3519–3532.
[18] J. DABIRI, S. COLIN AND J. COSTELLO, *Morphological diversity of medusan lineages constrained by animal-fluid interactions*, J. Experimental Bio., 210(11) (2007), pp. 1868–1873.
[19] D. T. RUDOLF, Jellyfish Through Numerical Simulation and Symmetry Exploitation, Ph.D. thesis, University of Saskatchewan, Saskatoon, SK, Canada, 2008.
[20] X. D. NIU, C. SHU, Y. T. CHEW AND Y. PENG, *A momentum exchange-based immersed boundary-lattice Boltzmann method for simulating incompressible viscous flows*, Phys. Lett. A, 354(3) (2006), pp. 173–182.
[21] S. CHEN AND G. D. DOOLEN, *Lattice Boltzmann method for fluid flows*, Annual Rev. Fluid Mech., 30 (1998), pp. 329–364.
[22] C. S. PESKIN, *Flow patterns around heart valves: a numerical method*, J. Comput. Phys., 10(2) (1972), pp. 252–271.
[23] J. PENG AND J. O. DABIRI, *Transport of inertial particles by lagrangian coherent structures: application to predator-prey interaction in jellyfish feeding*, J. Fluid Mech., 623 (2009), pp. 75–84.
[24] J. O. DABIRI, S. P. COLIN AND J. H. COSTELLO, *Fast-swimming hydromedusae exploit velar kinematics to form an optimal vortex wake*, J. Experimental Bio., 209(11) (2006), pp. 2025–2033.
[25] E. BULLARD, *Physical properties of sea water 2.7.9*, `http://www.kayelaby.npl.co.uk/general physics/27/279.html`, August 2010.
[26] M. D. FORD, J. H. COSTELLO, K. B. HEIDELBERG AND J. E. PURCELL, *Swimming and feeding by the scyphomedusa chrysaora quinquecirrha*, Marine Biology, 129 (1997), pp. 355–362.
[27] E. M. PURCELL, *Life at low Reynolds number*, Amer. J. Phys., 45(1) (1977), pp. 3–11.
[28] H. Z. YUAN, X. D. NIU, S. SHU, M. J. LI AND Y. HIROSHI, *A momentum exchange-based immersed boundary-lattice Boltzmann method for simulating a flexible filament in an incompressible flow*, Comput. Math. Appl., accepted, Jan 5, 2014.